The Structural and Magnetic ordering in $La_{0.5-x}Nd_xCa_{0.5}MnO_3$ ($0.1 \leq x \leq 0.5$) Manganites

Indu Dhiman[a], A. Das[a], P. K. Mishra[b], N. P. Lalla[c], and A. Kumar[a]

[a] *Solid State Physics Division, Bhabha Atomic Research Centre, Mumbai - 400085, India*
[b] *Technical Physics Division, Bhabha Atomic Research Centre, Mumbai - 400085, India*
[c] *UGC-DAE Consortium for Scientific Research, University Campus, Khandwa Road, Indore 452017, India*

Abstract

The crystal and magnetic structure of polycrystalline $La_{0.5-x}Nd_xCa_{0.5}MnO_3$ ($0.0 \leq x \leq 0.5$) samples have been investigated using magnetization, resistivity, transmission electron microscope, and neutron diffraction techniques. The samples are isostructural and possess orthorhombic structure in *Pnma* space group. On lowering of temperature, the samples exhibit CE - type antiferromagnetic structure coexisting with a weak ferromagnetic ordering. The charge and orbitally ordered antiferromagnetic phase is weakened by the growth of ferromagnetic phase. The evolution of structural distortions and magnetic structure at low temperature as a function of Nd doping exhibit a strong correlation with A - site disorder (σ^2).

Keywords: Manganites, Charge ordering, Phase separation, Neutron powder diffraction
PACS: 61.12.Ld, 75.25.+z, 75.50.-y, 75.47.Lx

1. Introduction

Half doped manganites $R_{0.5}A_{0.5}MnO_3$ (R: a trivalent earth ion, A: a divalent earth ion) have been attracting considerable interest due to strong coupling between the charge, spin, and orbitals. The charge and spin ordering in these compounds is highly sensitive to several perturbations such as disorder effects at the rare earth (A – site) and transition metal (B – site) site, hydrostatic pressure, magnetic and electric field, and size of the particles [1, 2, 3, 4]. In particular, substituting at A – site modifies the average A – site ionic radius $< r_A >$ and introduces disorder (σ^2) which is found to have significant influence on magnetic and transport properties. Disorder is expressed as $\sigma^2 = \sum x_i r_i^2 - < r_A >^2$, where x_i denotes the fractional occupancy of the A-site ion and r_i is the corresponding ionic radius and $< r_A >$ is the average A-site ionic radius [5].

Email address: adas@barc.gov.in (A. Das)

Half doped manganites with $< r_A > \sim 1.20 - 1.263$Å and disorder $\sigma^2 \sim 10^{-3} - 10^{-2}$ exhibit stable ferromagnetic phase coexisting with antiferromagnetic phase. Modifying the ionic radii with substitutions at the rare earth site generally leads to a suppression of the ferromagnetic phase. This is evidenced in the following studies. The influence of doping in systems such as $(Nd_{1-y}Sm_y)_{0.5}Sr_{0.5}MnO_3$ causes reduction in both T_C and T_{CO} [6]. In Y doped $Pr_{0.5}Sr_{0.5}MnO_3$ compound, the ferromagnetic phase is suppressed, while the antiferromagnetic transition temperature T_N either remains stable or shows a slight increase [7], whereas with Nd doping T_N shows a reduction and T_C remains nearly stable [8]. Magnetic and transport study of $La_{0.5-x}Ln_xSr_{0.5}MnO_3$ (Ln = Pr, Nd, Gd and Y) have shown a change over from ferromagnetic metallic state to an antiferromagnetic insulating phase with increase in x [9]. Similar studies on the effect of doping at the rare earth site in compounds with lower ionic radii $< r_A > \sim 1.14 - 1.20$Å and disorder $\sigma^2 \sim 10^{-6} - 10^{-4}$ have been investigated. Curiale et al. have studied the effect of Pr doping in $(La_yPr_{1-y})_{0.5}Ca_{0.5}MnO_3$ manganites and observe a rapid decline in ferromagnetic transition temperature T_C and increase of the charge ordering transition temperature (T_{CO}) [10]. In $Nd_{0.5-x}La_xCa_{0.5}MnO_3$ and $Pr_{0.5-x}La_xCa_{0.5}MnO_3$ systems the occurrence of a reentrant ferromagnetic state on cooling and a marked effect of disorder on T_C has been observed [11, 12, 13]. Most of these studies mainly focus on the influence of A – site disorder on magnetic transitions. The effect of disorder on the crystal and magnetic structure, including phase separation phenomenon, has not been studied widely.

The phase separation behaviour observed in half-doped manganites has also attracted wide theoretical interest [14, 15]. The appearance of a charge ordered CE-type antiferromagnetic ground state in manganites could not be reproduced using a superexchange model alone. The theoretical studies show that electron – phonon coupling (λ) due to cooperative or non-cooperative Jahn–Teller phonons in addition to double exchange and super exchange effects was necessary to reproduce the phase diagram of half-doped manganites with charge-orbitally ordered CE-type antiferromagnetic state [16, 17]. The random substitution of La^{3+} with Nd^{3+} ions may be identified with the quenched disorder. In the presence of quenched disorder the hopping of e_g electrons and the exchange interaction J_{AF} between t_{2g} spins is affected due to the buckling of Mn–O–Mn bonds. Taking into account the fluctuations of hopping and exchange couplings, Monte Carlo studies reveal the coexistence of giant clusters of ferromagnetic and antiferromagnetic phases [18]. Variation of disorder can lead to preferential stabilization of one phase as compared to the other. In a similar study, which included the electron – phonon coupling (λ), CE- and A-type antiferromagnetic and ferromagnetic phases were realized as a function of λ and J_{AF} [19].

The effect of A - site disorder on the nature of magnetic ordering in charge ordered manganites has been reported previously. However, in these studies the change in $<r_A>$ and σ^2 were significantly large [20, 21, 22, 23, 24, 25, 26]. In the present study we have investigated the influence of introducing very small disorder ($\sim 10^{-4}$) in $La_{0.5}Ca_{0.5}MnO_3$ compound. Towards this, we have studied compounds in the series $La_{0.5-x}Nd_xCa_{0.5}MnO_3$ ($0.1 \leq x \leq 0.5$). The end

compound $La_{0.5}Ca_{0.5}MnO_3$ ($<r_A>$ = 1.198Å) exhibits $T_C \approx 225$K, $T_{CO} \approx T_N \approx 170$K, having CE - type antiferromagnetic ground state with magnetic moment predominately oriented in the ac - plane [27], whereas in $Nd_{0.5}Ca_{0.5}MnO_3$ ($<r_A>$ = 1.17Å) ferromagnetic character is totally suppressed and it exhibits $T_{CO} \approx 240$K, $T_N \approx 150$K, CE - type antiferromagnetic ground state with moments oriented along a or c axis [28]. We find that introducing even a small disorder by susbstituting La with Nd in these class of compounds results in pronounced enhancement of micrometer size ferromagnetic clusters coexisting in an antiferromagnetic matrix.

2. Experimental Details

The polycrystalline samples were synthesized by conventional solid state reaction method. The starting materials La_2O_3, MnO_2, Nd_2O_3, and $CaCO_3$ were mixed in stoichiometric ratio and fired at 1200°C for 48hrs. Samples were then repeatedly ground and heated at 1400°C for 48hrs. Finally, the samples were pelletized and sintered at 1400°C for 60hrs. Initial values of cell parameters for all the samples were obtained from X-ray powder diffraction at 300K with a Rigaku diffractometer, rotating anode type using Cu Kα radiation. Neutron diffraction patterns were recorded on a multi PSD based powder diffractometer (λ = 1.249Å) at Dhruva reactor, Bhabha Atomic Research Centre, Mumbai at selected temperatures between 22 and 300K, in the $5^\circ \leq 2\theta \leq 140^\circ$ angular range. The powdered samples were packed in a cylindrical Vanadium container and attached to the cold finger of a closed cycle Helium refrigerator. Rietveld refinement of the neutron diffraction patterns were carried out using FULLPROF program [29]. Neutron depolarization measurements (λ = 1.205Å) were carried out on the polarized neutron spectrometer at Dhruva reactor, Bhabha Atomic Research Centre, Mumbai with Cu_2MnAl (1 1 1) as the polarizer and Co_2Fe (2 0 0) as analyzer. For transmission electron microscopy (TEM) studies the samples were prepared using conventional technique of ion milling at 3.3KV at 3° grazing incidence of the two Ar ion-guns. A LN_2 based double-tilt sample holder (636MA-Gatan) was used for carrying out low temperature TEM measurements, between 98 and 300K. The magnetization measurements were carried out using a SQUID magnetometer (Quantum Design, USA). The zero field (ZFC) and field cooled (FC) measurements were carried out in an external magnetic field H = 0.5T. Standard four probe technique was used to measure the dc resistivity between 3 and 300K.

3. Results and Discussion

3.1. Crystal structure and distortions

The Nd doped samples in the series $La_{0.5-x}Nd_xCa_{0.5}MnO_3$ ($0.1 \leq x \leq 0.5$) are isostructural and possess orthorhombic structure in *Pnma* space group. These compounds have perovskite structure with O´ orthorhombic insulating phase characterized by $b/\sqrt{2} \leq a \leq c$. In this structure cooperative Jahn – Teller

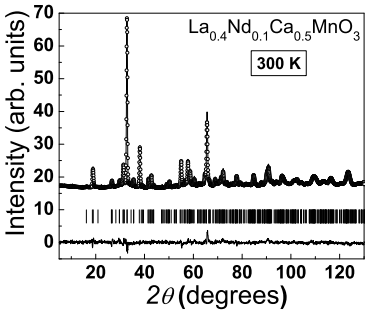

Figure 1: A representative neutron diffraction pattern for $La_{0.4}Nd_{0.1}Ca_{0.5}MnO_3$ (x = 0.1) sample at 300K. The continuous line through the data points is the Rietveld fit to the nuclear phase in *Pnma* space group. The vertical tick marks below the pattern corresponds to the indexing of the nuclear peaks in orthorhombic structure and curve at the bottom shows the difference between observed and calculated intensity.

distortions are superimposed on the rotation of MnO_6 octahedra [30, 31]. Volume exhibits nearly linear reduction as a function of Nd doping and is ascribed to a smaller ionic radius of Nd^{3+} ions in comparison to La^{3+} ions [32]. The structural parameters obtained from Rietveld refinement of neutron diffraction patterns at 300 and 22K are summarized in table I and II, respectively. The disorder albeit small, displays a maximum for intermediate composition in the range of x = 0.2 - 0.3.

Figure 1 shows the neutron diffraction pattern for x = 0.1 sample at 300K and Rietveld fit to the data. The values of lattice parameters obtained are consistent with the ones obtained from refinement of x – ray diffraction patterns at 300K and those reported in literature for the end compounds [27, 28]. On lowering of temperature below the charge ordering temperature T_{CO}, a structural transition to a lower symmetry monoclinic structure in space group $P2_1/m$ is expected, as has been reported in similar systems exhibiting charge ordering behavior [27]. We observe a signature of this in the form of splitting of nuclear Bragg reflections (2 4 2) (0 0 4) (4 0 0) below T_{CO}, as shown in figure 2. The selected portion of neutron diffraction pattern between $51.5^\circ \leq 2\theta \leq 56^\circ$ show that the splitting of nuclear Bragg reflections (2 4 2) (0 0 4) (4 0 0) in *Pnma* space group to ($\overline{4}$ 4 2) (4 4 2) and (8 0 0) in $P2_1/m$ space group occurs below 150K. This signifies the transformation of orthorhombic phase in *Pnma* space group to charge and orbitally ordered monoclinic phase in $P2_1/m$ space group. In $P2_1/m$ space group Mn^{3+} and Mn^{4+} ions occupy two distinct sites, in accordance with charge order scenario proposed in the Goodenough model [33]. However, the debate surrounding the charge disproportionation in the charge ordered state, between Goodenough [33] and Zener polaron [34, 35] model has not been settled yet in the literature. In the absence of high resolution data, we obtain similar

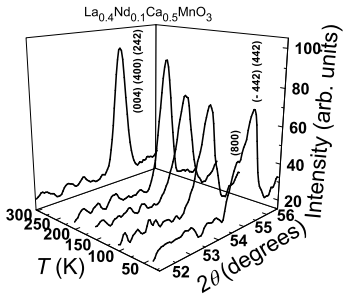

Figure 2: A selected portion ($51.5^\circ \leq 2\theta \leq 56^\circ$) of neutron diffraction patterns at various temperatures for $La_{0.4}Nd_{0.1}Ca_{0.5}MnO_3$ (x = 0.1) sample is shown. Splitting of (0 0 4) (4 0 0) (2 4 2) peak in *Pnma* space group to ($\overline{4}$ 4 2) (4 4 2) and (8 0 0) in $P2_1/m$ space group is evident at 22K, marking the orthorhombic to monoclinic structural transition.

values for χ^2 and R factors on fitting the diffraction pattern in both $P2_1/m$ and *Pnma* space groups. The lowering of symmetry to $P2_1/m$ space group requires refinement of 29 positional parameters. This reduces the reliability of refined positional parameters. Therefore, the low temperature crystal structure is refined in *Pnma* space group having 7 positional parameters, which yields an average structure as has been done in the case of x = 0 compound using neutron diffraction data [27]. In samples x = 0.2 and 0.3 with higher Nd doping, splitting attributable to the orthorhombic to monoclinic structural transition is reduced. This possibly indicates the modification of charge and orbital ordering in Nd doped samples. The TEM measurements discussed below display the presence of incommensurate charge ordering below 150K for x = 0.3 sample as against commensurate charge ordering observed for x = 0 sample [36]. In the Nd - rich end, the orthorhombic to monoclinic transition again becomes evident below 200 and 225K for x = 0.4 and 0.5 samples, respectively.

The temperature evolution of structural parameters, magnetization and resistivity for x = 0.1, 0.3, and 0.5 samples are shown in figures 3, 4, and 5, respectively. As temperature is reduced below 300K, the cell parameters, a and c exhibit a slight increase while b decreases drastically. This anomalous behavior of lattice parameters has also been observed in $La_{0.5}Ca_{0.5}MnO_3$ (x = 0) and is associated with the ordering of d_{z^2} orbitals in the a-c plane [27]. Similar behavior of cell parameters as a function of temperature is observed in samples with $x \leq 0.4$. The temperature dependent variation of lattice parameters in $Nd_{0.5}Ca_{0.5}MnO_3$ (shown in figure 5(a)) exhibits behavior similar to samples with $x \leq 0.4$, although the lattice parameter $a > c$ at all temperatures below 300K, in agreement with the previously reported study [28]. The Mn-O bond lengths as a function of temperature for samples x = 0.1, 0.3, and 0.5 are shown in figure 3(b), 4(b), and 5(b), respectively. In samples with $x \leq 0.2$, the differ-

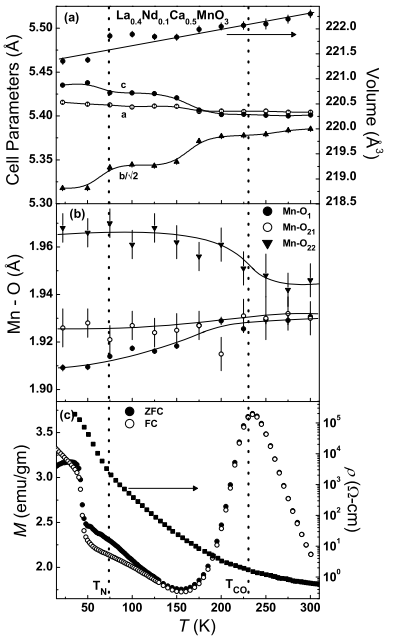

Figure 3: **(a)** Temperature dependence of lattice parameters and the unit-cell volume **(b)** Bond lengths as a function of temperature and **(c)** Variation of magnetization and resistivity as a function of temperature for $La_{0.4}Nd_{0.1}Ca_{0.5}MnO_3$ (x = 0.1) compound is shown. The continuous lines are a guide for the eye.

ence between three Mn – O bond lengths increases as temperature is reduced, indicating increase in distortion. However, in x = 0.3 sample, the Mn – O bond lengths exhibit no significant change as a function of temperature and remain very close to each other, indicating the suppression of JT distortions with the onset of ferromagnetic ordering. At higher doping with x $\geq$ 0.4, Mn – O bond lengths display behavior similar to samples with x $\leq$ 0.2. The temperature dependence of Mn-O bond lengths for sample x = 0.5 is shown in figure 5(b), and it exhibits behavior similar to x $\leq$ 0.2 samples. In contrast, the Mn-O-Mn bond angles remain nearly constant as a function of temperature in all the samples. To quantify the Mn-O bond length distortion, $\triangle_{JT} = \frac{1}{3}\sum\left[\left(d_n - d\right)/d_n\right]^2$ [29] as a function of Nd doping at 22K is calculated and are given in table II. The bond length distortion $\triangle_{JT}$ exhibits a minimum at x = 0.3 compound. The minimum in $\triangle_{JT}$ coincides with the minimum evident in charge ordering transition temperature (T_{CO}, obtained from the hump in magnetization) and resistivity values at 50K, for x = 0.3 sample. This indicates a close correlation between $\triangle_{JT}$, magnetic and transport properties and is in agreement with the

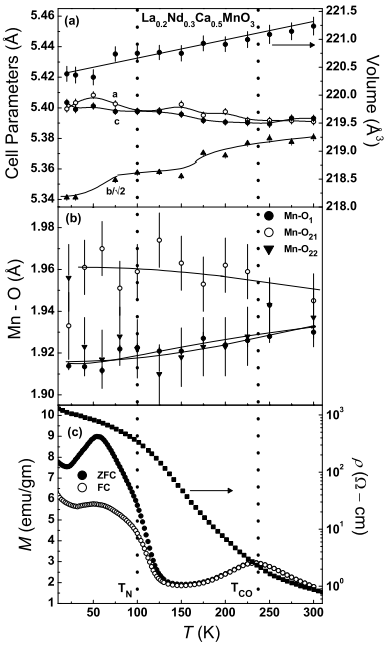

Figure 4: **(a)** Temperature dependence of lattice parameters and the unit-cell volume **(b)** Bond lengths as a function of temperature and **s** Variation of magnetization and resistivity as a function of temperature for $La_{0.2}Nd_{0.3}Ca_{0.5}MnO_3$ (x = 0.3) sample is shown. The continuous lines are a guide for the eye.

results from a similar study on the effect of Y doping in $Nd_{2/3}Ca_{1/3}MnO_3$ [38].

3.2. Magnetic and Transport Studies

The temperature dependence of magnetization, M(T), under zero field (ZFC) and field cooled (FC) conditions for x = 0.1, 0.3, and 0.5 samples at magnetic field H = 0.5T, are shown in figures 3(c), 4(c), and 5(c), respectively. The Nd doped samples undergo multiple magnetic transitions as a function of temperature. On reducing temperature below 300K a peak in magnetization at T = 235K is observed in the case of x = 0.1 sample. This coincides with the onset of charge ordered insulating transition and T_C as observed in x = 0 [55]. On further reduction of temperature a shoulder at T = 100K occurs, which we identify with antiferromagnetic ordering temperature, T_N. The nature of antiferromagnetic ordering below 100K is studied by neutron diffraction and is discussed below. Upon further cooling, M exhibits a sharp increase indicating another ferromagnetic transition at T = 45K. Although from neutron diffraction study no evidence for the presence of long range ferromagnetic ordering is observed

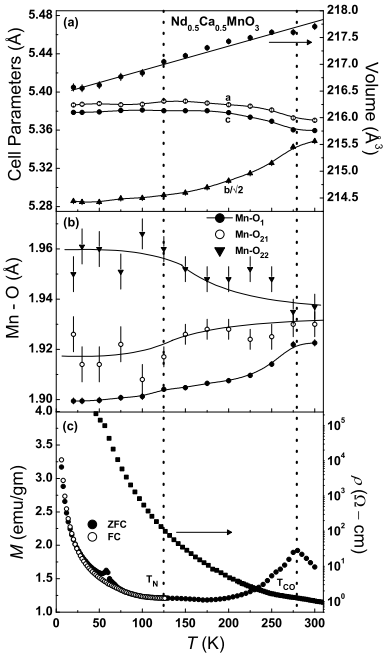

Figure 5: **(a)** Temperature dependence of lattice parameters and the unit-cell volume **(b)** Bond lengths as a function of temperature and **(c)** Variation of magnetization and resistivity as a function of temperature for $Nd_{0.5}Ca_{0.5}MnO_3$ (x = 0.5) sample is shown. The continuous lines are a guide for the eye.

in x = 0.1 sample. A magnetic transition coinciding with this temperature has been reported in $Nd_{1/2}Ca_{1/2}MnO_3$ sample, attributed to canted antiferromagnetic state [39, 40]. The canting angle in the present compounds may be too small to reflect changes in the neutron diffraction experiments. However, ferromagnetic nano clusters coexisting with the majority antiferromagnetic phase is also another possibility for the ferromagetic behavior in the antiferromagnetic state [41]. In addition, a bifurcation between ZFC and FC curves is observed at 120K. In all the samples with x $\leq$ 0.3, M(T) exhibits an anomalous behavior, the value of M in ZFC mode is higher than FC mode. Similar behavior has been observed in other charge ordered manganites, attributed to the development of ferromagnetic ordering below T_C that does not get completely suppressed in the antiferromagnetic state. Therefore, the system is blocked into a metastable state, a feature of the first order transition and phase separated state [42]. We understand that this phenomena is intrinsic to systems exhibiting charge ordering behavior. The transition to a charge ordered state is accompanied by a change in structure and therefore the resulting distortions are different across the transition. The difference between the ZFC and FC states essentially arises

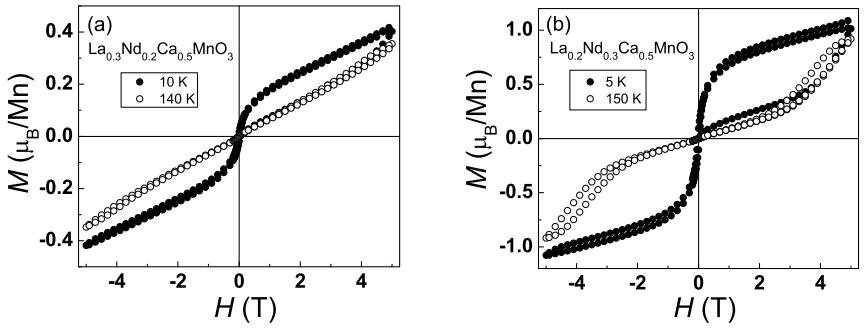

(a) x = 0.2 at 10 and 140K (b) for x = 0.3 at 5 and 150K

Figure 6: Variation of magnetization (M) with field (H) for $La_{0.5-x}Nd_xCa_{0.5}$-MnO_3 series having **(a)** x = 0.2 at 10 and 140K and **(b)** for x = 0.3 at 5 and 150K.

from application of magnetic field in crystallographically different structures. Magnetic field dependent dielectric studies carried out in charge ordered systems exhibit significant influence of magnetic field on the dielectric behavior, suggesting that the distortions are influenced by the magnetic field [43]. The peak temperature in M(T) identified as T_{CO} shows a minimum at x = 0.3 composition, coinciding with the minimum observed in the ($\triangle_{JT}$) distortion parameter. Furthermore, at very low temperature below 20K an appreciable increase in M(T) is observed. Such a behavior has been ascribed to a magnetic contribution due to Nd^{3+} sublattice. This becomes stronger and in the case of $Nd_{1/2}Ca_{1/2}MnO_3$ this tail extends to a much higher temperature [28]. At higher Nd concentration (x $\geq$ 0.4), the difference in M(T) for ZFC and FC mode is considerably reduced, indicating the absence of ferromagnetic character. This is in agreement with previously reported magnetization study on $Nd_{1/2}Ca_{1/2}MnO_3$ compound [28].

The variation of magnetization with field, M(H), for samples x = 0.2 and 0.3 are shown in figures 6(a) and (b), respectively. At low temperatures (10K for x = 0.2 and 5K for x = 0.3) the M(H) displays a narrow hysteresis loop and a large slope at high fields in M(H), suggesting the coexistence of ferromagnetic and antiferromagnetic phases. Additionally, anomalous behavior in the form of virgin curve lying outside the envelop curve for both x = 0.2 and 0.3 and a step like behavior only for x = 0.3 sample is visible. The steps are sharp at low temperatures and shifts to higher fields and becomes less distinct with increase in temperature. High resolution neutron diffraction studies carried out in presence of field have found that the step in M(H) in charge ordered systems with CE type antiferromagnetic structure is accompanied by a change in the cell parameters [44, 45]. Magnetic field as high as 6T is found to increase the ferromagnetic character, but the CE-type antiferromagnetic structure almost remains undisturbed in $Pr_{0.5}Ca_{0.5}Mn_{0.97}Ga_{0.03}O_3$ compound. A similar

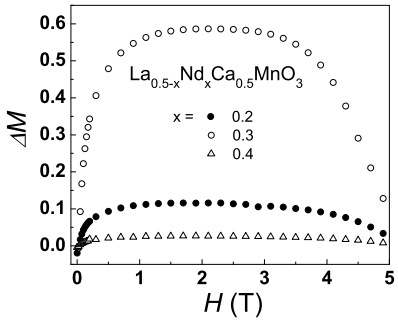

Figure 7: Difference of magnetization on the envelope and virgin curve as a function of field for $La_{0.5-x}Nd_xCa_{0.5}MnO_3$ series having x = 0.2, 0.3, and 0.4.

description based on martensitic like scenario on the strain accomodation in phase separated manganites has been proposed to explain the step like behavior in M(H) [45, 46]. The appearance of sharp metamagnetic steps in M(H) is attributed to the presence of different crystallographic unit cell of phase separated antiferromagnetic and ferromagnetic regions. At low temperatures, the coexistence of ferromagnetic regions in an antiferromagnetic matrix results in an elastic constraint effects at the interface. When the applied magnetic field favoring the growth of ferromagnetic regions become large enough to overcome the elastic constraints, it causes a sudden jump in magnetization. As a consequence of these elastic constraints, the ferromagnetic regions cannot grow continuously. Fisher et al. have shown that the quenched disorder induces an inhomogeneous metastable state and subsequent magnetization jumps in $(SmSr)MnO_3$ [47]. At T = 140K in x = 0.2 sample, the M(H) exhibits a linear behavior in the paramagnetic regime, while in x = 0.3 sample at 150K a narrow hysteresis loop is still evident, suggesting the presence of short range ordered ferromagnetic state. In x = 0.4 sample, the M(H) at 10K shows an extremely narrow hysteresis loop and a feature of virgin curve lying outside the envelope curve, while at 140K the M(H) exhibits a linear field dependence. The behavior of virgin curve lying outside the envelope curve has also been interpreted in terms of kinetically arrested first order phase transition and the associated features like phase coexistence and metastability [48]. The extent to which the virgin curve lies outside envelope curve is decided by the initial conditions of two competing phases (ferromagnetic and antiferromagnetic) in the H-T phase space. A larger fraction of ferromagnetic phase surviving metastably to zero field, upon field reversal would cause a larger difference between virgin and envelope curves [49]. This is illustrated in figure 7, where the difference between virgin and envelope curves is plotted as a function of Nd concentration. The difference is maximum in x = 0.3 in comparison to x = 0.2 and 0.4 samples. This indicates that in x = 0.3 sample a larger fraction of the ferromagnetic state persists metastably to zero field upon field reversal. Therefore, at low temperature all three samples show

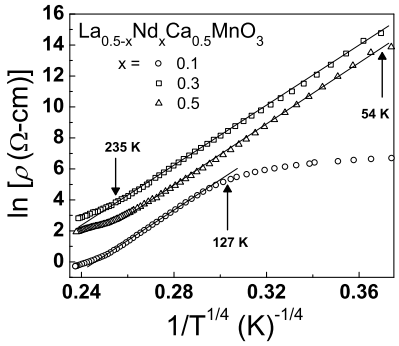

Figure 8: Plot of ln ρ versus temperature $T^{-1/4}$ for x = 0.1, 0.3 and 0.5 samples. The curve for x = 0.5 sample is shifted artificially to enhance clarity.

the presence of ferromagnetic clusters in an antiferromagnetic matrix, although the fraction / size of these clusters is significantly larger in x = 0.3 sample.

The temperature dependence of resistivity, ρ(T), in x = 0.1, 0.3 and 0.5 compositions are shown in figures 3(c), 4(c), and 5(c), respectively. The resistivity data were collected during heating and cooling cycles. Thermal hysteresis was not observed between the two cycles. For all the Nd doped samples temperature dependence of resistivity shows an insulating behavior over the entire measured temperature range between 50 and 315K. Below 50K resistivity is too high to be measurable. No significant change in ρ(T) with Nd doping is observed except for x = 0.3 sample. In this sample reduction in resistivity by nearly two orders of magnitude is observed in comparison to other Nd doped samples and is, shown in figure 4(c). The decrease in ρ(T) for x = 0.3 sample can be attributed to the presence of ferromagnetic regions. In literature various models have been proposed to explain the conduction mechanism in charge ordered manganites. In the temperature regime below T_{CO} the resistivity behavior is best described by Mott's variable range hopping model. We find, the conduction process in systems with localized effects is described using the variable range hopping (VRH) model. In this model ρ(T) is expressed as [50],

$$\rho = \rho_0 \exp\left(T_0/T\right)^{1/4}$$

where, T_0 is the Mott's activation energy, and is defined as $T_0 \approx \frac{21}{K_B N(E_F)\xi^3}$. In this equation, k_B is Boltzmann constant, $N\left(E_F\right)$ is the density of states at Fermi level, and ξ is the localization length. The characteristic temperature T_0 is related to the electronic density of states at the Fermi level. The ln ρ versus $T^{-1/4}$ plot for samples x = 0.1, 0.3 and 0.5 is shown in figure 8. For clarity the plot for x = 0.5 sample is artificially shifted. The temperature range of fitting is considerably reduced and shows a deviation from variable range hopping model below ∼130K in x = 0.3 sample. This behavior may be ascribed

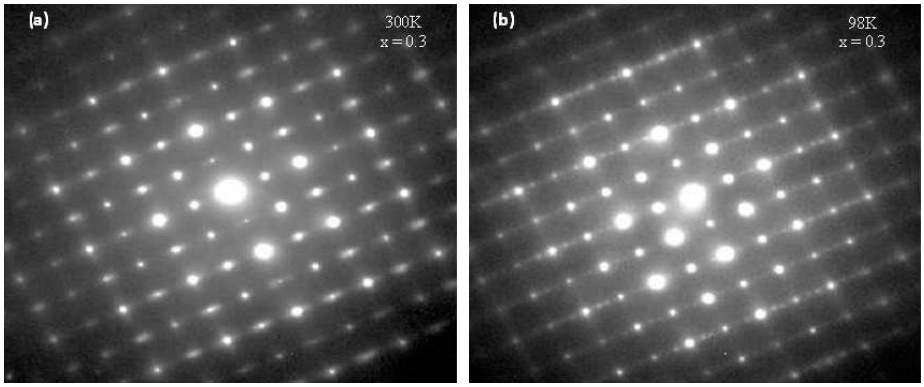

(a) at 300K (b) at 98K

Figure 9: Selected area diffraction patterns for $La_{0.2}Nd_{0.3}Ca_{0.5}MnO_3$ (x = 0.3) compound at **(a)** 300K and **(b)** 98K.

to the presence of ferromagnetic interactions in addition to charge and orbitally ordered antiferromagnetic phase at low temperatures. No significant change in the value of T_0 as a function of Nd doping is evident. The value of T_0 for x = 0.1, 0.3 and 0.5 samples are 0.544 (9) $\times 10^8 K$, 0.87 (2) $\times 10^8 K$ and 1.15 (8) $\times 10^8 K$, respectively. The value of T_0 for the end compound $Nd_{0.5}Ca_{0.5}MnO_3$ (x = 0.5) is fairly in agreement with the value ($T_0 \approx 3.4{\times}10^8 K$) reported in literature [28]. In contrast with previously reported transport and magnetization studies on $Nd_{0.5-x}La_xCa_{0.5}MnO_3$ series [11], we do not observe metal to insulator transition in these samples though a reduction in resistivity by two orders of magnitude in x = 0.3 sample is found.

3.3. TEM studies

The influence of Nd doping on charge and orbitally ordered structure in x = 0.3 and 0.4 sample is investigated using TEM measurements. Electron diffraction patterns and high resolution lattice images were recorded at various temperatures between 98 and 300K. In both Nd doped samples with x = 0.3 and 0.4, electron diffraction patterns exhibit identical *Pnma* structure, showing a typical 90° - domains of orthorhombic structure in *Pnma* space group. At 300K diffuse streaks along a* (the reciprocal-space lattice parameter) are observed and indicate a signature of high temperature charge – orbitally ordered fluctuations, as shown in figure 9(a) for x = 0.3 sample. The presence of such fluctuations at 300K therefore lead to an approximate *Pnma* structure. In the temperature region above T_{CO}, we have found evidence of short range order using diffuse neutron scattering studies in related compounds, $La_{0.5}Ca_{0.5-x}Sr_xMnO_3$ [23], which corroborates with the present TEM observation. As temperature is reduced below 300K down to 220K, no significant difference between the selected area diffraction patterns is observed. On further reducing the temperature to 150K, the short range charge ordered fluctuations is enhanced, leading to an onset of long range incommensurate charge and orbitally ordered phase. At

98K, the electron diffraction pattern shows the presence of relatively intense superlattice spots at positions between the Bragg peaks corresponding to *Pnma* structure and is shown in figure 9(b). These superlattice spots can be indexed as q = (1/3 – ε)a*, where ε is the parameter of incommensurability. By taking into account the orientation of e_g orbitals of Mn^{3+} ions, the lattice parameter along a-axis is doubled leading to corresponding superlattice spots. Thus it is the orbital ordering, in combination with charge-ordering, which causes the superlattice spots [36]. No transition from incommensurate to commensurate charge ordering structure is observed down to 98K. Unlike in $La_{0.5}Ca_{0.5}MnO_3$ (x = 0) compound, the temperature dependent TEM study reveals that the ferromagnetic to antiferromagnetic transition is accompanied by a incommensurate to commensurate charge ordering transition at 130K [36]. In x = 0.4 sample, similar incommensurate charge ordered phase is observed at 98K. Although, in comparison to x = 0.3 sample the superlattice spots have much higher intensity, which indicates the strengthening of charge ordered phase. The occurrence of incommensuration in Nd doped samples indicate the presence of charge itinerancy, therefore weakening of antiferromagnetic state.

3.4. Magnetic Structure

The neutron diffraction pattern of x = 0.1 sample at 300 and 22K in the angular range of $5^\circ \leq 2\theta \leq 70^\circ$ is shown in figure 10(a) and (b), respectively. This neutron diffraction pattern is representative for all the samples. On lowering of temperature below the respective antiferromagnetic ordering temperatures superlattice reflections are observed, similar to that of x = 0 sample, indicating the antiferromagnetic nature of samples [27]. The values of refined magnetic moment on Mn site at 22K and antiferromagnetic ordering temperature are given in table II. The superlattice reflections are marked with an asterisks (*) symbol in figure 10(b). Particularly, reflections (0, 1, $\frac{1}{2}$) ($\frac{1}{2}$, 1, $\frac{1}{2}$) and (1, 1, $\frac{1}{2}$) are shown and these characterize the onset of a CE – type antiferromagnetic state. These superlattice reflections are indexed on a 2a × b × 2c cell in the space group $P2_1/m$. In CE – type antiferromagnetic spin structure Mn occupies two distinct sites for Mn^{3+} and Mn^{4+} ions. The Mn^{3+} and Mn^{4+} sublattices are associated with propagation vector (0, 0, $\frac{1}{2}$) and ($\frac{1}{2}$, 0, $\frac{1}{2}$), respectively [27]. In this structure, zig zag ferromagnetic chains are coupled antiferromagnetically within and out of plane. The model was first proposed by Wollan and Kohler [51]. Unlike in the case of Y doped samples [52], the CE - type antiferromagnetic structure is stable over the entire range of composition. Though, in the intermediate composition, where the disorder is maximum, the antiferromagnetic moment is considerably reduced. The temperature dependence of magnetic moment for x = 0.1 sample is shown in the inset of figure 10(b). The Rietveld refinement of the neutron diffraction pattern at 22K indicates that the magnetic moment for Mn^{3+} and Mn^{4+} sites are predominantly oriented along either a or c axis and have values as 2.5(2) μ_B and 2.2(1) μ_B, respectively. From the present neutron diffraction data no significant change in χ^2 and magnetic R - factor is observed on changing the orientation of spins between a and c axis, and therefore spins were constrained to be orientated along a axis. Similarly, the x and z component

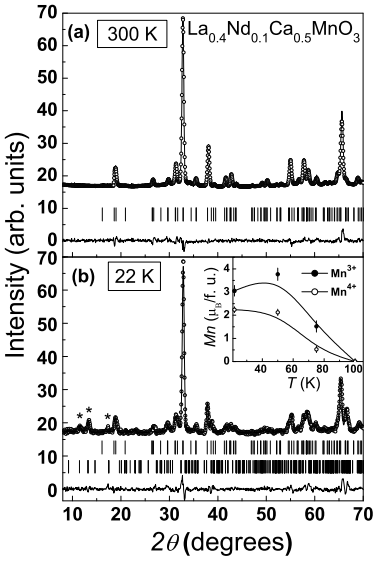

Figure 10: Neutron diffraction pattern recorded on sample $La_{0.4}Nd_{0.1}Ca_{0.5}MnO_3$ (x = 0.1) at **(a)** 300 and **(b)** 22K. This figure is representative for all the samples having x $\leq$ 0.5. Continuous line through the data points is the fitting to chemical and magnetic structure described in the text. The (*) symbols indicate superlattice reflections having maximum intensity in the CE-type antiferromagnetic state. The vertical tick marks below the diffraction pattern in **(a)** correspond to positions of Bragg reflections. While in **(b)** the upper and lower tick marks indicate the indexing of nuclear and CE-type antiferromagnetic phases, respectively. The inset of figure **(b)** shows the variation of antiferromagnetic site moment of Mn^{3+} and Mn^{4+} ions with temperature for sample x = 0.1. The continuous lines are a guide for the eye.

of magnetic moment of Mn^{4+} ions could not be refined separately, and therefore the orientation was constrained to be along c axis. This behavior is similar to the previously reported neutron diffraction study on $La_{0.5}Ca_{0.5}MnO_3$ compound by Radaelli et al. [27]. With Nd doping the reorientation of spins from ac plane to either a or c axis is observed. In addition, no enhancement of intensity in low angle fundamental Bragg reflections was visible, which indicates the absence of ferromagnetic ordering from the present neutron diffraction experiment. Nevertheless, the M(H) and M(T) study at low temperature for x = 0.2 and 0.3 samples show signatures for the presence of ferromagnetism, indicating the moment values are too small to influence the neutron diffraction data. However, evidence of ferromagnetic behavior in agreement with M(T) measurements is found using neutron depolarization measurements, discussed below. Therefore,

M(H) in conjunction with M(T), neutron diffraction, and neutron depolarization studies indicate the presence of phase separation behavior, with coexisting ferromagnetic and antiferromagnetic phases particularly for x = 0.3 composition. For the end compound $Nd_{0.5}Ca_{0.5}MnO_3$ (x = 0.5) the refinement of low temperature pattern clearly indicates that the magnetic moments are oriented along a axis. The value of moments for Mn^{3+} and Mn^{4+} are 2.4(1) μ_B and 1.8(1) μ_B at 22K, with the transition temperature $T_N \approx 125$K. In contrast, according to previously reported neutron diffraction study on $Nd_{0.5}Ca_{0.5}MnO_3$ compound the $T_N \approx 160$K, which is higher than our reported value [28].

3.5. Neutron Depolarization

The temperature dependence of magnetization in the anitferromagnetic state in samples x $\leq$ 0.3 exhibits an increase in magnetization on lowering of temperature indicating presence of coexisting ferromagnetic and antiferromagnetic phases. This behavior is further probed using neutron depolarization measurements. This technique measures spatial magnetic inhomogeneities on a length scale from 1000Å to several micrometers. In the present study, we have measured flipping ratio R (ratio of the transmitted intensities for two spin states of the incident neutron spin), which is a measure of the transmitted beam polarization. R is expressed in the form ,

$$R = \frac{1 - P_i D P_A}{1 + (2f - 1) P_i D P_A}$$

where, P_i is the incident beam polarization, P_A is the efficiency of the analyzer crystal, f is the rf flipper efficiency and D is the depolarization coefficient. In the absence of any depolarization in sample, $D = 1$. $P_i D$ is thus the transmitted beam polarization. As against M(H) measurements, where the sample is subjected to high field, depolarization measurements provide information about the presence of ferromagnetic domains in low magnetic fields and therefore, does not disturb the magnetic ground state. Hence, depolarization measurement is advantageous to study the ferromagnetic behavior in samples with coexisting ferromagnetic and antiferromagnetic phases.

Figure 11 shows the temperature dependence of transmitted neutron beam polarization in a field of 32 Oe, for x = 0.2 and 0.3 samples. In other samples depolarization is not observed down to lowest temperature. For x = 0.2 a very small change in transmitted beam polarization is observed below 150K. In contrast to x = 0.2 sample, the x = 0.3 compound displays a significant depolarization below 125K, becoming nearly constant for T $<$ 50K indicating presence of ferromagnetic domains. The ferromagnetic nature in x = 0.2 and 0.3 samples observed from neutron depolarization studies explains the increase in magnetization in the antiferromagnetic state below 150K observed in figure 5(c). An estimate of domain size in the ferromagnetic region is obtained using the expression $P_f = P_i exp(-\alpha(d/\delta)) < \phi_\delta >^2$ where, P_f and P_i are the transmitted beam and incident beam polarization, respectively, α is a dimensionless parameter (= 1/3), d is the sample thickness, δ is a typical domain

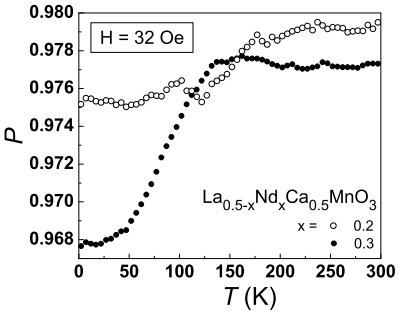

Figure 11: Temperature dependence of transmitted neutron beam polarization (P) for $La_{0.5-x}Nd_xCa_{0.5}MnO_3$ (x = 0.2 and 0.3) in H = 32 Oe is displayed.

length and the precession angle $\phi_\delta = (4.63 \times 10^{-10} Oe^{-1} \mathring{A}^{-2})\lambda\delta B$ [53]. The domain magnetization, B is obtained from the bulk magnetization. This expression is valid in the limit where domains are randomly oriented and the Larmor phase of neutron spin due to the internal magnetic field of sample $< 2\pi$ over a typical domain length scale. Our measurements were carried out in low field far away from the saturation field and therefore satisfy the assumption of this model. The estimated domain size for x = 0.3 sample at T = 2K is $\sim 0.1\mu m$. For higher Nd doping (x = 0.4), behavior similar to x = 0.2 sample is observed. The absence or low value of depolarization indicates reduction in ferromagnetic domain size and / or domain magnetization. This measurement therefore, gives a clear evidence of ferromagnetic domains coexisting in the antiferromagnetic state. The absence of contribution to the Bragg reflections in the low temperature neutron diffraction studies indicates that the long range ferromagnetic ordering is absent. Previously, evidence of nano clusters of ferromagnetic origin in the charge ordered antiferromagnetic state has been reported [41]. Here, we provide the evidence of fairly large ferromagnetic domains in the charge ordered antiferromagnetic state induced by disorder. Monte Carlo studies show that nano sized ferromagnetic clusters in antiferromagnetic phase arise in the electronically phase separated state where the densities of ferromagnetic and antiferromagnetic phases are unequal [15]. In the case where the densities are equal, disorder σ^2 is found to cause large micrometer size ferromagnetic domains in the antiferromagnetic matrix, which is evidenced from the present depolarization studies. Experimentally, coexistence of ferromagnetic and antiferromagnetic phase has been reported in $La_{0.5}Ca_{0.5}MnO_3$ [41, 54]. As against, the previous studies, we find that increase in disorder leads to larger size ferromagnetic domains in antiferromagnetic matrix, which is in agreement with theoretical studies on phase separation behavior in charge ordered manganites [15].

Thus, based on the results presented here it is observed that upon moderate increase in disorder with Nd doping (x < 0.3), the charge and orbitally ordered

ground state is not fully suppressed. Simultaneously a ferromagnetic phase is found to grow, leading to a coexistence of ferromagnetic and antiferromagnetic phases at low temperature. Moreover, the stepwise behavior evident in M(H) for x = 0.3 sample corresponds to field induced diminution of charge and orbitally ordered antiferromagnetic phase and growth of ferromagnetic phase. These effects are commonly observed in phase separated systems. Radaelli et al. have shown that for parent compound (x = 0) the charge and orbitally ordered phase is accompanied by an increase of ac strain [55]. With induced disorder the homogeneous strain field is collapsed into an inhomogeneous one (as a result of Nd substitution), which is accompanied by the gradual reduction of charge ordered phase. Theoretical studies have shown that long range homogenous strain plays a crucial role in stabilization of charge and orbitally ordered state in half doped manganites. Ahn et al. have reported that the presence of uniform strain favors stabilization of the charge ordered phase [56]. Recently, the significance of lattice strain and in turn the influence of disorder on strain field has been further elucidated in studies of bulk as well as in thin films of half doped manganites [57, 58, 59, 60, 61]. In thin films it has been shown that epitaxial strain could have a strong effect on charge ordered state. Therefore, both the interior and exterior strains are of substantial importance in stabilizing charge and orbitally ordered phase. For higher Nd doping (x $\geq$ 0.4), with reducing disorder the ferromagnetic phase is fully suppressed while the charge ordered antiferromagnetic phase is favored. This behavior is in agreement with increase in Jahn Teller distortions (Δ_{JT}) for x $\geq$ 0.4 samples. Hence, a strong correlation of small disorder with structural and magnetic behavior is evident.

4. Conclusion

We have investigated the influence of small A – site disorder ($\sim 10^{-4}$) on magnetic and transport behavior of charge and orbitally ordered $La_{0.5-x}Nd_x$-$Ca_{0.5}MnO_3$ ($0.0 \leq x \leq 0.5$) series. The disorder as a function of Nd doping displays a maximum in the range of x = 0.2 - 0.3 compositions. The Nd doped compounds possess orthorhombic structure in space group $Pnma$ at room temperature and on reducing temperature below T_{CO} exhibit a transition to lower symmetry monoclinic structure in $P2_1/m$ space group. The compounds undergo antiferromagnetic transition between 100 and 125K. Below T_N the magnetic structure is CE-type. Evidence of ferromagnetic domains coexisting with the CE-type antiferromagnetic ordering is found in the neutron depolarization and magnetization measurements. The estimated domain size in x = 0.3 sample at T = 2K is $\sim 0.1\mu m$. The growth of ferromagnetic phase exhibits a maximum for x = 0.3 compound. The Jahn – Teller distortion (Δ_{JT}) parameter exhibits a minimum for x = 0.3 compound. The growth of ferromagnetic state results in reduction in resistivity, though insulator to metal transition is not observed in the Nd doped samples. Therefore, the evolution magnetic and nuclear structure at low temperatures as a function of Nd doping exhibit strong correlation even with small A - site disorder (σ^2).

Table 1: Structural parameters obtained from Rietveld refinement of neutron diffraction pattern at 300K for samples $La_{0.5-x}Nd_xCa_{0.5}MnO_3$. The atomic sites are: La/Nd/Ca 4c[x, 1/4, z]; Mn 4a[0, 0, 0]; O_1 4c[x, 1/4, z]; O_2 8d[x, y, z] in Pnma space group. The symbol O_1 denotes the Oxygen atom along b axis (apical) and O_{21} and O_{22} are the two Oxygen atoms in the ac-plane (equatorial).

Refined parameters		x = 0.1	x = 0.2	x = 0.3	x = 0.4	x = 0.5
a (Å)		5.404 (1)	5.399 (1)	5.391 (2)	5.395 (2)	5.3703 (9)
b (Å)		7.616 (1)	7.607 (1)	7.609 (3)	7.608 (4)	7.564 (1)
c (Å)		5.401 (1)	5.392 (1)	5.393 (2)	5.374 (2)	5.3595 (9)
V ($Å^3$)		222.30 (8)	221.50 (8)	221.2 (2)	220.6 (1)	217.71 (6)
$<r_A>$		1.1927	1.1874	1.1821	1.1768	1.1715
$\sigma^2 \times 10^{-4}$		3.8	3.92	3.41	2.35	0.723
La/Nd/Ca	x	0.020 (1)	0.018 (1)	0.014 (2)	0.026 (2)	0.0292 (8)
	z	0.490 (2)	0.500 (5)	0.484 (3)	0.496 (4)	0.493 (2)
O_1	x	0.493 (2)	0.495 (3)	0.499 (4)	0.481 (2)	0.488 (1)
	z	0.559 (2)	0.565 (2)	0.557 (3)	0.569 (3)	0.564 (1)
O_2	x	0.278 (1)	0.277 (1)	0.287 (2)	0.281 (2)	0.284 (1)
	y	0.0319 (8)	0.030 (9)	0.032 (2)	0.031 (1)	0.0349 (7)
	z	0.220 (2)	0.222 (2)	0.213 (3)	0.219 (2)	0.2145 (9)
$Mn - O_1$ (Å)		1.931 (1)	1.935 (2)	1.927 (3)	1.941(3)	1.923(1)
$Mn - O_{21}$ (Å)		1.930 (7)	1.931 (8)	1.943 (13)	1.933 (10)	1.930 (5)
$Mn - O_{22}$ (Å)		1.946 (7)	1.935 (8)	1.943 (14)	1.932 (11)	1.937 (5)
$Mn - O_1 - Mn$ (°)		160.91 (7)	158.74 (8)	161.1 (1)	157.1 (1)	159.20 (6)
$Mn - O_2 - Mn$ (°)		160.5 (3)	161.6 (4)	157.7 (6)	160.1 (4)	157.7 (2)

Table 2: Structural parameters obtained from Rietveld refinement of neutron diffraction pattern at 22K for samples $La_{0.5-x}Nd_xCa_{0.5}MnO_3$. The atomic sites are: La/Nd/Ca 4c[x, 1/4, z]; Mn 4a[0, 0, 0]; O_1 4c[x, 1/4, z]; O_2 8d[x, y, z] in Pnma space group. The symbol O_1 denotes the Oxygen atom along b axis (apical) and O_{21} and O_{22} are the two Oxygen atoms in the ac-plane (equatorial).

Refined parameters		x = 0.1	x = 0.2	x = 0.3	**x** = 0.4	x = 0.5
a (Å)		5.415 (1)	5.396 (1)	5.399 (2)	5.406 (1)	5.386 (1)
b (Å)		7.5203 (9)	7.556 (1)	7.554 (2)	7.519 (1)	7.475 (4)
c (Å)		5.435 (1)	5.421 (1)	5.403 (2)	5.401 (1)	5.379 (1)
V ($Å^3$)		221.35 (7)	221.04 (8)	220.4 (1)	219.56 (9)	216.57 (7)
La/Nd/Ca	x	0.020 (1)	0.024 (2)	0.016 (2)	0.036 (1)	0.0292 (9)
	z	0.496 (3)	0.492 (2)	0.485 (2)	0.489 (1)	0.491 (1)
O_1	x	0.488 (2)	0.487 (2)	0.503 (3)	0.483 (1)	0.487 (1)
	z	0.561 (1)	0.562 (1)	0.557 (2)	0.559 (1)	0.562 (1)
O_2	x	0.273 (1)	0.271 (2)	0.285 (3)	0.279 (1)	0.281 (1)
	y	0.0357(4)	0.0329 (7)	0.0316 (9)	0.0348 (6)	0.0354 (5)
	z	0.223 (3)	0.223 (2)	0.211 (3)	0.224 (1)	0.216 (1)
$\Delta_{JT} \times 10^{-4}$		1.6 (4)	1.2 (6)	0.8 (3)	1.0 (4)	1.2 (4)
T_N (K)		100	100	100	125	125
M (μ_B)						
μ_x (Mn^{3+})		2.5 (2)	0.8 (4)	1.7 (3)	2.6 (2)	2.5 (2)
μ_x (Mn^{4+})		2.2 (1)	0.9 (1)	0.6 (2)	2.2 (1)	1.8 (1)
$Mn - O_1$ (Å)		1.909 (1)	1.921 (2)	1.914 (2)	1.908 (1)	1.899 (1)
$Mn - O_{21}$ (Å)		1.926 (8)	1.913 (10)	1.933 (16)	1.954 (7)	1.926 (7)
$Mn - O_{22}$ (Å)		1.968 (6)	1.961 (10)	1.956 (2)	1.927 (8)	1.950 (7)
$Mn - O_1 - Mn$ (°)		159.97 (5)	159.18 (7)	161.32 (7)	160.14 (5)	159.38 (5)
$Mn - O_2 - Mn$ (°)		160.2 (3)	161.6 (4)	158.3 (7)	159.8 (3)	158.2 (3)

References

[1] C. N. R. Rao and B. Raveau, Colossal Magnetoresistance, Charge Ordering, and Related Properties of Manganese Oxides World Scientific, 1998, Singapore.

[2] E. Dagotto, Nanoscale Phase Separation and Colossal Magnetoresistance, Springer Series in Solid State Physics Vol. 136 Springer, 2003, Berlin.

[3] J. B. Goodenough, in Handbook on the Physics and Chemistry of Rare Earth, edited by K. A. Gschneidner, Jr., J.-C. Bunzli, and V. K. Pecharsky Elsevier Science, Vol. 33, 2003, Amsterdam.

[4] Y. Tokura, Rep. Prog. Phys. 69 (2006) 797.

[5] L. M. Rodriguez-Martinez and J. P. Attfield, Phys. Rev. B 54 (1996) R15622, L. M. Rodriguez-Martinez and J. P. Attfield, Phys. Rev. B 58 (1998) 2426.

[6] H. Kuwahara, Y. Moritomo, Y. Tomioka, A. Asamitsu, M. Kasai, R. Kumai and Y. Tokura, Phys. Rev. B 56 (1997) 9386.

[7] J. Wolfman, Ch. Simon, M. Hervieu, A. Maignan, B. Raveau, J. Solid State Chem. 123 (1996) 413.

[8] L. S. Ling, S. Tan, L. Pi and Y. H. Zhang, Europhys. Lett. 79 (2007) 47008.

[9] Md. Motin Seikh, L. Sudheendra, and C. N. R. Rao, J. Solid State Chem. 177 (2004) 3633.

[10] J. Curiale, C. A. Ramos, P. Levy, R. D. Sanchez, F. Rivadulla, and J. Rivas, Physica B 354 (2004) 47.

[11] P. V. Vanitha and C. N. R. Rao, J. Phys.: Condens. Matter 13 (2001) 11707.

[12] D. Zhu, X. Tan, P. Cao, F. Jia, X. Ma, and Y. Lu, J. Appl. Phys. 105 (2009) 063914.

[13] S. Yang, J. Zhong, J. Miao, J. Yuan, B. Xu, L. Cao, X. Qiu, B. Zhao, Z. Xie, and L. Zhao, Physica B 370 (2005) 99.

[14] A. Moreo, S. Yunoki and E. Dagotto, Science 283 (1999) 2034.

[15] E. Dagotto, T. Hotta, A. Moreo, Phys. Rep. 344 (2001) 1.

[16] J. van den Brink, G. Khaliullin and D. Khomskii, Phys. Rev. Lett. 83 (1999) 5118.

[17] L. Brey, Phys. Rev. B 71 (2005) 174426.

[18] A. Moreo, M. Mayr, A. Feiguin, S. Yunoki and E. Dagotto, Phys. Rev. Lett. 84 (2000) 5568.

[19] K. Pradhan, A. Mukherjee and P. Majumdar, Phys. Rev. Lett. 99 (2007) 147206.

[20] A. Das, P. D. Babu, Sandip Chatterjee and A. K. Nigam, Phys. Rev. B 70 (2004) 224404,

[21] P. D. Babu, A. Das, S. K. Paranjpe, Solid State Commun. 118 (2001) 91.

[22] I. Dhiman, A. Das, P. K. Mishra, and L. Panicker, Phys. Rev. B 77 (2008) 094440,

[23] I. Dhiman, A. Das, R. Mittal, Y. Su, A. Kumar, and A. Radulescu, Phys. Rev. B 81 (2010) 104423.

[24] I. Dhiman, A. Das and A. K. Nigam, J. Phys.: Condens. Matter 21 (2009) 386002.

[25] C. Autret-Lambert, Z. Jirak, M. Gervais, N. Poirot, F. Gervais, N. Raimboux, P. Simon, F. Boure, and G. Andr, Chem. Mater. 19 (2007) 5222.

[26] S. Savitha Pillai, G. Rangarajan, N. P. Raju, A. J. Epstein and P. N. Santhosh, J. Phys.: Condens. Matter 19 (2007) 496221.

[27] P. G. Radaelli, D. E. Cox, M. Marezio and S. -W. Cheong, Phys. Rev. B 55 (1997) 3015.

[28] F. Millange, S. de Brion, and G. Chouteau, Phys. Rev. B 62 (2000) 5619.

[29] J. Rodriguez-Carvajal, Physica B 192 (1993) 55.

[30] B. B. Van Aken, O. D. Jurchescu, A. Meetsma, Y. Tomioka, T. Tokura, and T. T. M. Palstra, Phys. Rev. Lett. 90 (2003) 066403.

[31] G. Maris, V. Volotchaev and T. T. M. Palstra, New J. Phys. 6 (2004) 153.

[32] A-site cationic radii for ninefold coordination in oxides were taken from R. D. Shannon, Acta Crystallogr., Sect. A: Cryst. Phys., Diffr., Theor. Gen. Crystallogr., A32 (1976) 751.

[33] J. B. Goodenough, Phys. Rev. 100 (1955) 564.

[34] A. Daoud-Aladine, J. Rodríguez-Carvajal, L. Pinsard-Gaudart, M. T. Fernández-Díaz, and A. Revcolevschi, Phys. Rev. Lett. 89 (2002) 097205.

[35] L. Wu, R. F. Klie, Y. Zhu, and Ch. Jooss, Phys. Rev. B 76 (2007) 174210.

[36] C. H. Chen and S. -W. Cheong, Phys. Rev. Lett. 76 (1996) 4042.

[37] J. Rodríguez-Carvajal, M. Hennion, F. Moussa, A. H. Moudden, L. Pinsard, and A. Revcolevschi, Phys. Rev. B 57 (1998) 3189(R).

[38] E. Fertman, A. Beznosov, D. Sheptyakov, V. Desnenko, M. Kajnakova, A. Feher and D. Khalyavin, J Magn. Magn. Mater. 321 (2008) 316.

[39] T. Vogt, A. K. Cheetham, R. Mahendiran, A. K. Raychaudhuri, R. Mahesh and C. N. R. Rao, Phys. Rev. B 54 (1996) 15303.

[40] P. Murugavel, C. Narayana, A. K. Sood, S. Parashar, A. R. Raju and C. N. R. Rao, Europhys. Lett. 52 (2000) 461.

[41] J. C. Loudon, N. D. Mathur, and P. A. Midgley, Nature London 420 (2002) 19.

[42] L. Ghivelder and F. Parisi, Phys. Rev. B 71 (2005) 184425.

[43] C. R. Serrao, A. Sundaresan, and C. N. R. Rao, J. Phys.: Condens. Matter 19 (2007) 496217.

[44] C. Yaicle, C. Martin, Z. Jirak, F. Fauth, G. Andre, E. Suard, A. Maignan, V. Hardy, R. Retoux, M. Hervieu, S. Hebert, B. Raveau, Ch. Simon, D. Saurel, A. Brulet, and F. Bouree, Phys. Rev. B 68 (2003) 224412.

[45] V. Hardy, S. Hebert, A. Maignan, C. Martin, M. Hervieu, and B. Raveau, J. Magn. and Magn. Mater. 264 (2003) 183.

[46] V. Hardy, C. Yaicle, S. Hebert, A. Maignan, C. Martin, M. Hervieu, and B. Raveau, J. Appl. Phys. 94 (2003) 5316.

[47] L. M. Fisher, A. V. Kalinov, I. F. Voloshin, N. A. Babushkina, D. I. Khomskii, Y. Zhang, T. T. M. Palstra, Phys. Rev. B 70 (2004) 212411.

[48] A. Banerjee, K. Mukherjee, K. Kumar and P. Chaddah, Phys. Rev. B 74 (2006) 224445, A. Banerjee, A. K. Pramanik, K. Kumar and P. Chaddah, J. Phys.: Condens. Matter 18 (2006) L605.

[49] M. A. Manekar and S. B. Roy, Eur. Phys. J. B 64 (2008) 19.

[50] N. F. Mott and E. A. Davis, Electronic Processes in Non Crystalline Materials 2^{nd} edn. 1979 (Oxford: Clarendon).

[51] E.O. Wollan and W.C. Kohler, Phys. Rev. 100 (1955) 545.

[52] E. Pollert, S. Krupicka, E. Kuzmicova, J. Phys. Chem. Solids 43 (1982) 1137.

[53] G. Halperin and T. Holstein, Phys. Rev. 59 (1941) 960 , R. W. Erwin, J. Appl. Phys. 67 (1990) 5229.

[54] Q. Huang, J. W. Lynn, R. W. Erwin, A. Santoro, D. C. Dender, V. N. Smolyaninova, K. Ghosh, and R. L. Greene, Phys. Rev. B 61 (2000) 8895.

[55] P. G. Radaelli, D. E. Cox, M. Marezio, S.-W. Cheong, P. E. Schiffer, and A. P. Ramirez, Phys. Rev. Lett. 75 (1995) 4488.

[56] K. H. Ahn, T. Lookman, and A. R. Bishop, Nature (London) 428 (2004) 401.

[57] P. Wagner, I. Gordon, A. Vantomme, D. Dierickx, M. J. Van Bael, V. V. Moshchalkov, and Y. Bruynseraede, Europhys. Lett. 41 (1998) 49.

[58] W. Prellier, A. Biswas, M. Rajeswari, T. Venkatesan, and R. L. Greene, Appl. Phys. Lett. 75 (1999) 397.

[59] X. J. Chen, S. Soltan, H. Zhang, and H.-U. Habermeier, Phys. Rev. B 65 (2002) 174402.

[60] X. J. Chen, H.-U. Habermeier, and C. C. Almasan, Phys. Rev. B 68 (2003) 132407.

[61] X. J. Chen, H. -U. Habermeier, H. Zhang, G. Gu, M. Varela, J. Santamaria, and C. C. Almasan, Phys. Rev. B 72 (2005) 104403.